

Review

Synthesis of fullerene nanowhiskers using the liquid–liquid interfacial precipitation method and their mechanical, electrical and superconducting properties

Kun'ichi Miyazawa

Fullerene Engineering Group, Materials Processing Unit, National Institute for Materials Science, Tsukuba, Ibaraki 305-0044, Japan

E-mail: miyazawa.kunichi@nims.go.jp

Received 27 November 2014, revised 14 January 2015

Accepted for publication 16 January 2015

Published 25 February 2015



CrossMark

Abstract

Fullerene nanowhiskers (FNWs) are thin crystalline fibers composed of fullerene molecules, including C_{60} , C_{70} , endohedral, or functionalized fullerenes. FNWs display *n*-type semiconducting behavior and are used in a diverse range of applications, including field-effect transistors, solar cells, chemical sensors, and photocatalysts. Alkali metal-doped C_{60} (fullerene) nanowhiskers (C_{60} NWs) exhibit superconducting behavior. Potassium-doped C_{60} NWs have realized the highest superconducting volume fraction of the alkali metal-doped C_{60} crystals and display a high critical current density (J_c) under a high magnetic field of 50 kOe. The growth control of FNWs is important for their success in practical applications. This paper reviews recent FNWs research focusing on their mechanical, electrical and superconducting properties and growth mechanisms in the liquid–liquid interfacial precipitation method.

Keywords: fullerene nanowhisker, fullerene nanotube, fullerene nanosheet, fullerene nanofiber, LLIP method, superconductor


1. Introduction

Fullerene molecules consist of closed cage-type structures that are composed of carbon atoms. The best-known fullerene is C_{60} , which was discovered by Kroto *et al* in 1985 [1]. The second well-known molecule is C_{70} , which was also identified in [1]. The C_{60} molecule is analogous to a soccer ball with 12 pentagons and 60 vertices where carbon atoms are located, and has 30 six-membered ring/six-membered ring joints with double bonds of carbon and 60 five-membered ring/six-membered ring joints with single bond of carbon.

Polymerization of C_{60} molecules can occur via [2+2] cycloaddition reactions, which form four-membered rings between adjacent C_{60} molecules. This cycloaddition mechanism involves a change of carbon hybridization from sp^2 to sp^3 [2].

Various properties of C_{60} have been studied by forming thin films on suitable substrates. Bulk samples can also be prepared by sintering at high temperatures. The [2+2] cycloaddition polymerization of C_{60} molecules is known to occur in the presence of ultraviolet or visible light illumination [3, 4], high-pressure sintering [5–8], and electron beam irradiation [9, 10]. The hardness of high-pressure sintered C_{60} reaches 200–300 GPa [11, 12].

However, fine needle-like crystals (whiskers) comprising C_{60} , ‘ C_{60} (fullerene) nanowhiskers (C_{60} NWs)’, were found in

 Content from this work may be used under the terms of the [Creative Commons Attribution 3.0 licence](https://creativecommons.org/licenses/by/3.0/). Any further distribution of this work must maintain attribution to the author(s) and the title of the work, journal citation and DOI.

a colloidal solution of lead zirconate titanate (PZT) with C_{60} added [13–15].

Fullerene nanofibers are linear and thin, with diameters less than 1000 nm [16, 17]. Fullerene nanosheets are thin two-dimensional substances. In this paper, we define fullerene nanosheets to be less than 1000 nm in thickness. Fullerene nanofibers and nanosheets can include a variety of fullerene molecules and their derivatives including C_{60} , C_{70} , $Sc_3N@C_{80}$ [18], $C_{60}[C(COOC_2H_5)_2]$ [19–21] and $(\eta^2-C_{60})Pt(PPh_3)_2$ [22].

The aspect ratio of fullerene nanofibers is defined to be greater than three [16]. Fullerene nanofibers are described as either non-tubular or tubular [23–27]. Non-tubular crystalline fullerene nanofibers are called fullerene nanowhiskers (FNWs). FNWs with both single-crystal and polycrystalline structures have been reported [53].

Fullerene nanofibers can incorporate either one or multiple types of fullerenes. This enables formation of both monocomponent and multicomponent structures. Examples of monocomponent structures include C_{60} NWs, C_{70} (fullerene) nanowhiskers (C_{70} NWs), C_{60} or C_{70} (fullerene) nanotubes (C_{60} NTs or C_{70} NTs), [23, 25, 28], and FNWs composed of $C_{60}[C(COOC_2H_5)_2]$ molecules ($C_{60}[C(COOC_2H_5)_2]$ NWs). Examples of multicomponent fullerene nanofibers include two-component C_{60} – C_{70} NWs [29], two-component C_{60} – C_{70} NTs [23], two-component C_{60} – $C_{60}[C(COOC_2H_5)_2]$ NWs [19], and two-component C_{60} – $(\eta^2-C_{60})Pt(PPh_3)_2$ NWs [22]. Figure 1 shows the classification of fullerene nanofibers.

Fullerene nanofibers and nanosheets can be synthesized using the ‘liquid–liquid interfacial precipitation (LLIP) method’ [30], which has been widely applied [31–38]. In this review, we discuss the LLIP method to synthesize fullerene nanofibers and nanosheets and the applications in which these materials have been investigated.

The terminology ‘FNW’ represents all needle-like crystals comprising fullerene molecules with diameters less than 1000 nm. The words ‘nanorod’ and ‘nanowire’ are replaced with ‘nanowhisker’ to avoid confusion as was described in review paper [16].

2. Synthesis of FNWs

2.1. LLIP method

The LLIP method is commonly used to synthesize fullerene nanofibers and nanosheets [30]. This method relies on diffusion of a poor solvent of fullerenes such as isopropyl alcohol (IPA) into a fullerene-saturated toluene solution. An aliquot of a C_{60} -saturated toluene solution is added to a glass bottle. Following this, an appropriate amount of IPA is added gently to the solution to form a liquid–liquid interface [8]. The resulting mixture is kept at ambient temperatures, typically below 25 °C. During the slow mixing of toluene and IPA, the liquid–liquid interface becomes supersaturated in C_{60} and allows nucleation of C_{60} NWs to occur. This supersaturated state is maintained as IPA diffuses into toluene and assists in

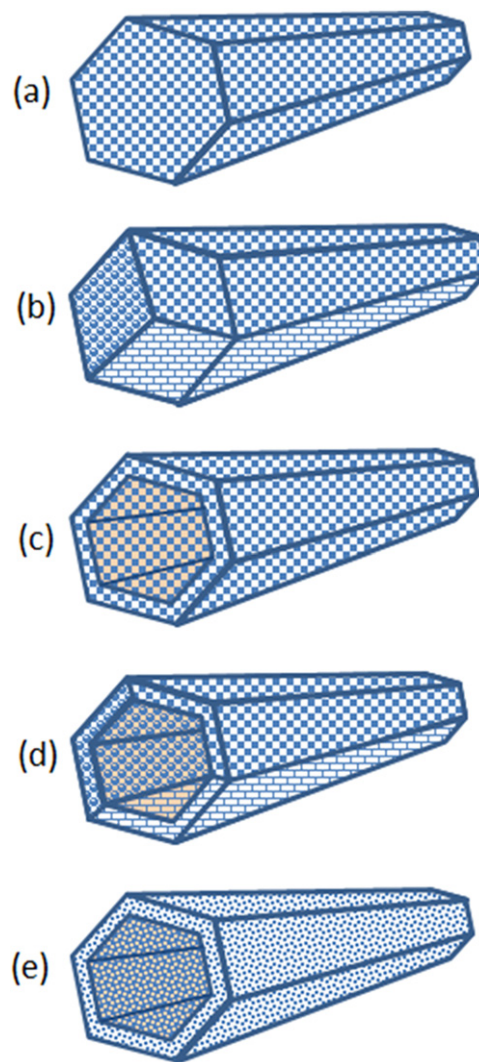


Figure 1. Classification of fullerene nanofibers. (a) single-crystal fullerene nanowhisker, (b) polycrystal fullerene nanowhisker, (c) single-crystal fullerene nanotube, (d) polycrystal fullerene nanotube, (e) amorphous fullerene nanotube.

the growth of C_{60} NWs. This procedure is named ‘static LLIP method’ [30, 39]. The glass bottle is kept still in an incubator, where the C_{60} NWs self-assemble into a shape similar to a cotton ball. The LLIP method can also be used in combination with ultrasonic mixing, manual mixing, or injection [24, 39, 40]. Ultrasonication induces rapid mixing of good solvents and poor solvents, causing formation of fine fullerene nuclei that grow into fullerene nanofibers or nanosheets.

The static LLIP method can involve layering a poor solvent onto a good solvent or vice versa, and can be combined with manual mixing, supersonic mixing, mixing by injection of liquid, or ultrasonic mixing of liquid droplets [41]. These methods are collectively named the ‘dynamic LLIP method’.

Cha *et al* and Miyazawa *et al* reported the diaphragm LLIP method (DLLIP method), which involves injecting a poor solvent for fullerene into a fullerene solution through a porous membrane [40, 42, 43]. As an example, if IPA is slowly injected into a C_{60} -saturated toluene solution through

an anodic aluminum oxide membrane with nanosized pores, vertically grown microtubes of C₆₀ are produced. All methods that mix two solvents to form fullerene nanofibers and nanosheets can be classified as LLIP processes.

Using the DLLIP method, the influence of alcohol chain length (methanol, ethanol, and IPA) on the length of C₆₀ whiskers was investigated using toluene as a good solvent for C₆₀. Amer *et al* reported that the length of C₆₀ whiskers decreased when the chain length of the alcohol (poor solvent) increased [44]. The temperatures at which the C₆₀ whiskers were grown was not reported; however, the above result suggests that the chain length of the alcohol influences the desolvation energy of solvated C₆₀ molecules that governs the rate-limiting process of surface reaction [45].

2.2. Growth mechanism of FNWs using the LLIP method

The Young modulus of C₆₀NWs has been examined using a transmission electron microscope equipped with an atomic force microscope [46]. The Young modulus of C₆₀NWs increases with decreasing diameter [46–49]. This phenomenon is thought to occur because C₆₀NWs have a core–shell structure with a porous interior region and a dense surface region [48, 50]. Kizuka *et al* found that C₇₀NWs containing solvent molecules had a higher density of lattice defects in their interior regions, which caused a reduction in the Young modulus [51]. Additionally, the Young modulus of C₇₀NTs was found to increase with decreasing diameter [25]. These studies conclude that by decreasing the diameter of fullerene nanofibers, crystallinity is increased, which in turn leads to an increase in the Young modulus.

In the LLIP process, FNWs grow from seed crystals [52–54]. The size of the initial C₆₀NW nuclei is influenced by the degree of supersaturation of C₆₀ in solution, which is determined by the mixing ratio of both good and poor solvents [39]. C₆₀NTs grow in both directions along their growth axis from the seed crystals [53, 54]. However, the seed crystals should disappear by the core dissolution mechanism to form a through-hole structure [55].

The re-growth of C₆₀NTs was observed in ultrasonically pulverized C₆₀NTs [53]. The ultrasonically fractured C₆₀NTs have steep wall edges, on which C₆₀ molecules accumulate and crystallize [53]. This preferential accumulation of C₆₀ in areas with a small radius of curvature, such as the hexagonal vertices, is an important growth mechanism of fullerene nanotubes [53, 54].

The growth of C₆₀NWs is influenced by numerous factors, including time, temperature, light, solvent species, the ratio between good and poor solvents, and contained impurity water [39, 56–59]. The growth mechanism of C₆₀NWs in C₆₀-saturated toluene and IPA has been studied closely. The activation energy of growth (52.8 kJ mol⁻¹) was calculated by varying the temperature and measuring the length of C₆₀NWs. This value is approximately four times greater than the value obtained for the diffusion of C₆₀ in a mixed solution of toluene and acetonitrile (13.1 kJ mol⁻¹, 4:1 v/v) [56, 60]. The high activation energy indicated that the growth of C₆₀NWs is

rate limited by the desolvation process of C₆₀ molecules bonded with solvent molecules on the crystal surface.

The dynamic LLIP process involves a fullerene solution being forcibly mixed with a poor solvent for fullerene. This process generates microscopic liquid–liquid interfaces between the fullerene solution and the poor solvent of fullerene, where supersaturated solutions lead to rapid nucleation of fine fullerene crystals. The formation of granular, linear, or sheet fullerene crystal morphologies depends on the growth kinetics, which may be governed by the degree of supersaturation, solvent species, and temperature.

Size control of fullerene nanofibers is critical for practical applications. Wakahara *et al* reported that the diameter of C₆₀NWs varied with the size of the glass bottles used in their synthesis. Linear relationships between the area of the liquid–liquid interface and the diameter of C₆₀NWs were observed when the total volume of solution was fixed [61]. Changes in the lengths and diameters of C₆₀NWs upon varying the solution volume have been examined [62]. These C₆₀NWs were prepared by dynamic LLIP in a C₆₀-saturated toluene and IPA system. After the initial formation of a liquid–liquid interface by layering an equal amount of IPA on a C₆₀-saturated toluene solution, the solution was manually mixed by shaking 30 times. The relationships between solution volume and mean length, diameter and aspect ratio are shown in figures 2(a)–(c) [62]. The aspect ratio, as derived from the *y*-intercepts of figures 2(a) and (b) (5.02 μm/387 nm) yielded a value of 13.0, almost identical to the value derived from the *y*-intercept of figure 2(c) (13.1). Hence, it is reasonable to consider the size of C₆₀NW nuclei can be estimated using the relationships shown in figures 2(a)–(c).

The relationship between the solution volume and number of C₆₀NWs per unit volume is shown in figure 2(d). The number density, as calculated from the nominal content of C₆₀ and the mean size of C₆₀NWs in solution [62], increased as the solution volume decreased. This implies that the volume fraction of liquid–liquid interfaces increases when the solution volume is decreased. A power law relationship ($y = 1.12 \times 10^9 x^{-0.567}$) was fitted to the data with an approximate index of -0.5, showing that the number density of C₆₀NW nuclei in solution is inversely proportional to the square root of the solution volume.

A model describing the changes in the liquid–liquid interface upon manual mixing is shown in figure 3. The initial layered interface (figure 3(a)) is assumed to form a sinusoidally modulated interface (figure 3(b)) upon the manual mixing. The amplitude of this interface increases along the height of the glass bottle, a section of this wavefront is highlighted by the blue rectangle (figure 3(c)). This highlighted section is modeled by a cylinder with height *h*, radius *r*, basal area *S*, and volume *V* (figure 4(a)). The front of the liquid–liquid interface travels vertically with a velocity *v*.

The following equations hold.

$$V = Sh, \quad (1)$$

$$h = pr, \text{ where } p \text{ is a constant,} \quad (2)$$

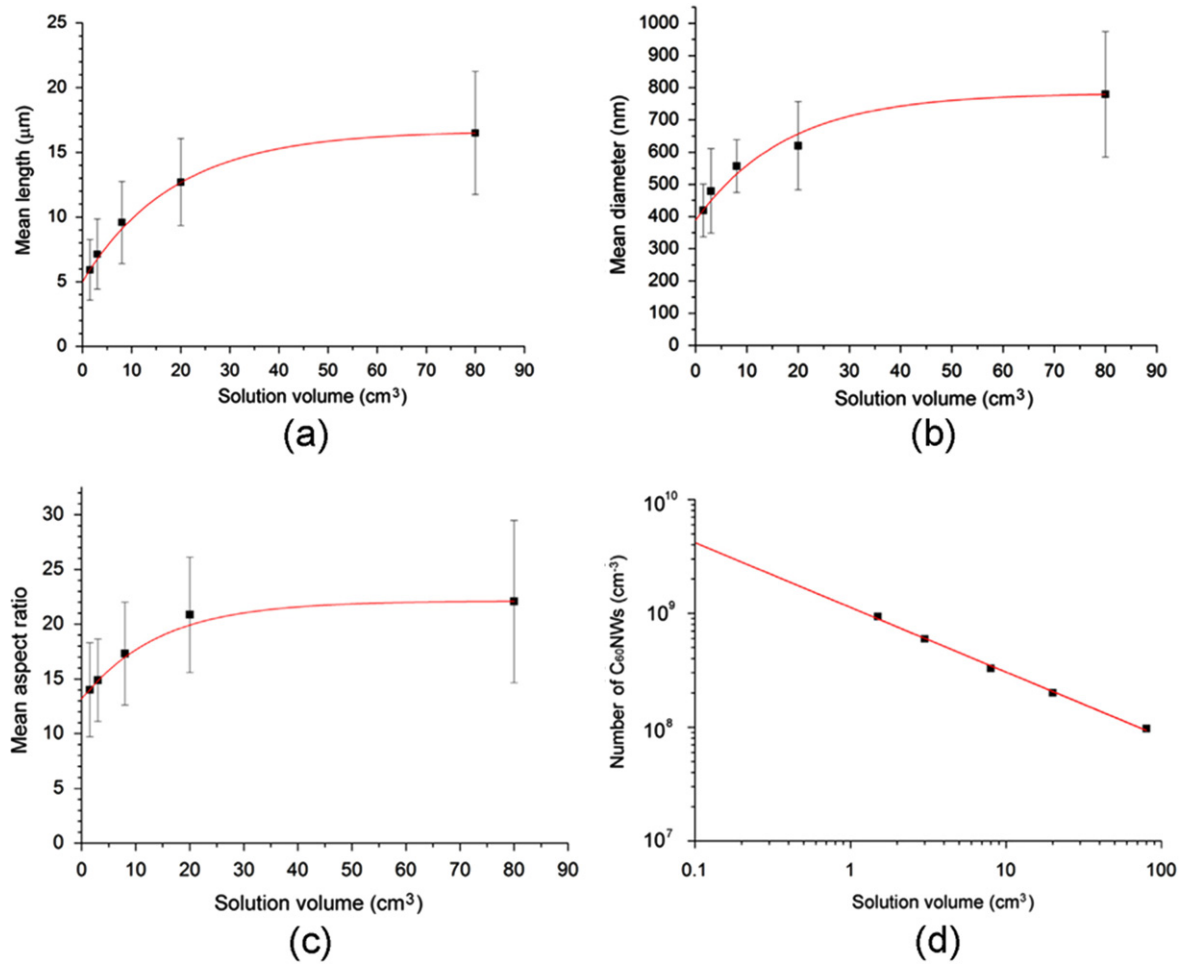


Figure 2. (a) Relationship between solution volume and mean length of C₆₀NWs. The equation fitted to the data is $y = -11.6\exp(-x/18.7) + 16.6$. (b) Relationship between solution volume and mean diameter of C₆₀NWs. The equation fitted to the data is $y = -396.6\exp(-x/17.6) + 783.7$. (c) Relationship between solution volume and the mean aspect ratio of C₆₀NWs. The equation fitted to the data is $y = -9\exp(-x/14.2) + 22.1$. (d) Estimated number of C₆₀NWs per unit volume plotted versus the solution volume. The equation fitted to the data is $y = -1.12496 \times 10^9 x^{-0.5674}$. Reprinted from [62], copyright 2014, with permission from Elsevier.

$$V = qS^{3/2}, \text{ where } q = p/\pi^{1/2}. \quad (3)$$

The front of liquid–liquid interface is assumed to move along the height h with a time t .

$$t = h/\nu. \quad (4)$$

As the liquid–liquid interface front moves, interdiffusion between C₆₀-saturated toluene solution and IPA occurs (figure 4(b)). If the values of both t and Δr are assumed to be small, the area of the interdiffusion zone (ΔS) is approximated as follows:

$$\Delta S = 2\pi r\Delta r. \quad (5)$$

The volume of interdiffusion ΔV is:

$$\Delta V = h\Delta S. \quad (6)$$

If Δr is assumed to be proportional to $(Dt)^{1/2}$ with a coefficient of interdiffusion D [63], it is calculated as in equation (7) with a constant a ,

$$\Delta r = at^{1/2}. \quad (7)$$

Hence, combining (4), (5), and (7),

$$\Delta S = bh^{1/2}, \text{ where } b = 2\pi ra(1/\nu)^{1/2}. \quad (9)$$

If N is defined as the number of C₆₀NW nuclei per unit volume in the zone of interdiffusion, the mean number of C₆₀NW nuclei contained in a unit volume of a cylinder (ρ) can be calculated by combining equations (1), (3), (6), and (9):

$$\rho = (Nbq)V^{-1/2}. \quad (12)$$

This model suggests that the mean number density of C₆₀NW nuclei is inversely proportional to the square root of the solution volume, which was indeed confirmed experimentally (figure 2(d)).

3. Electrical and superconducting properties of C₆₀NWs

C₆₀NWs display n -type semiconducting behavior and are used in a diverse range of applications, including field effect

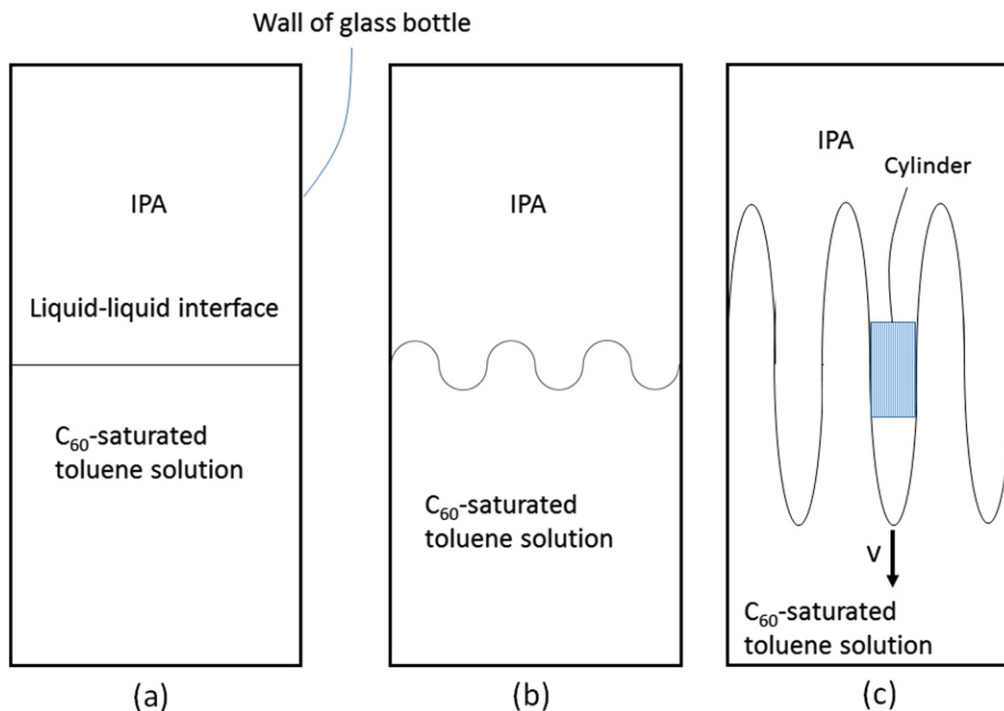


Figure 3. Model showing the liquid–liquid interface (a) changing with manual mixing (b). The interface front between the C₆₀-saturated toluene solution and IPA is assumed to move with a velocity v along the vertical direction of the glass bottle (c).

Initial position of liquid-liquid interface

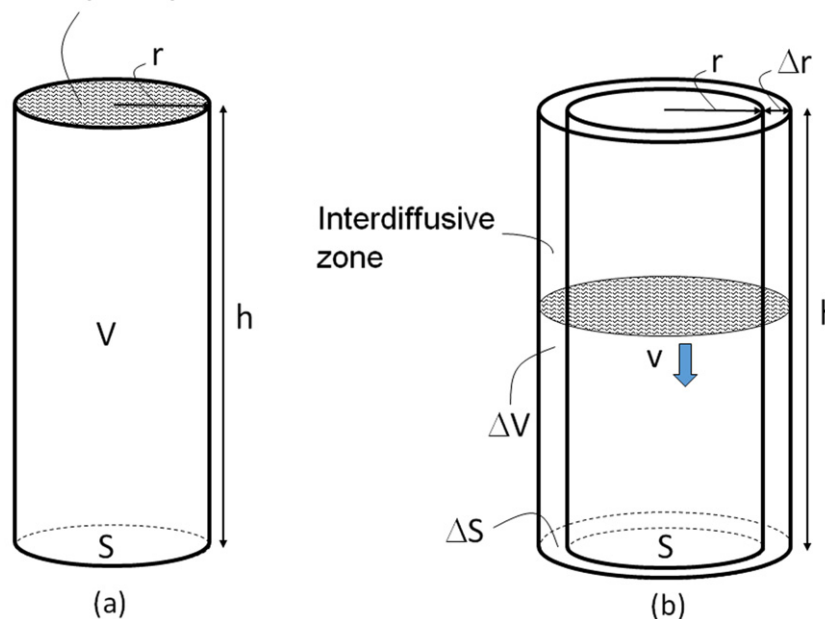


Figure 4. Cylindrical model used to calculate the number density N of C₆₀NW nuclei for the region of the liquid–liquid interface shown in figure 3(c).

transistors (FETs) [64], solar cells [65, 66], photocatalysts [67], chemical sensors [27], and photosensors [68]. However, Wakahara *et al* recently synthesized ambipolar FETs with C₆₀/cobalt–porphyrin hybrid nanosheets using a LLIP method [92].

The carrier mobility of C₆₀NWs in a FET was determined to be $2 \times 10^{-2} \text{ cm}^2 \text{ V}^{-1} \text{ s}^{-1}$ under vacuum [64]. However, the as-synthesized solution-grown C₆₀ needle-like crystals

exhibited a very high mobility up to $11 \text{ cm}^2 \text{ V}^{-1} \text{ s}^{-1}$ [69]. As the measured carrier mobility of C₆₀NWs, or needle-like crystals of C₆₀, depends largely on the measurement conditions (solvent impurities, oxygen impurity, crystal structure, and lattice defects), electrical properties of the materials were investigated under controlled conditions. Only C₆₀NWs with clearly defined chemical and structural properties were used.

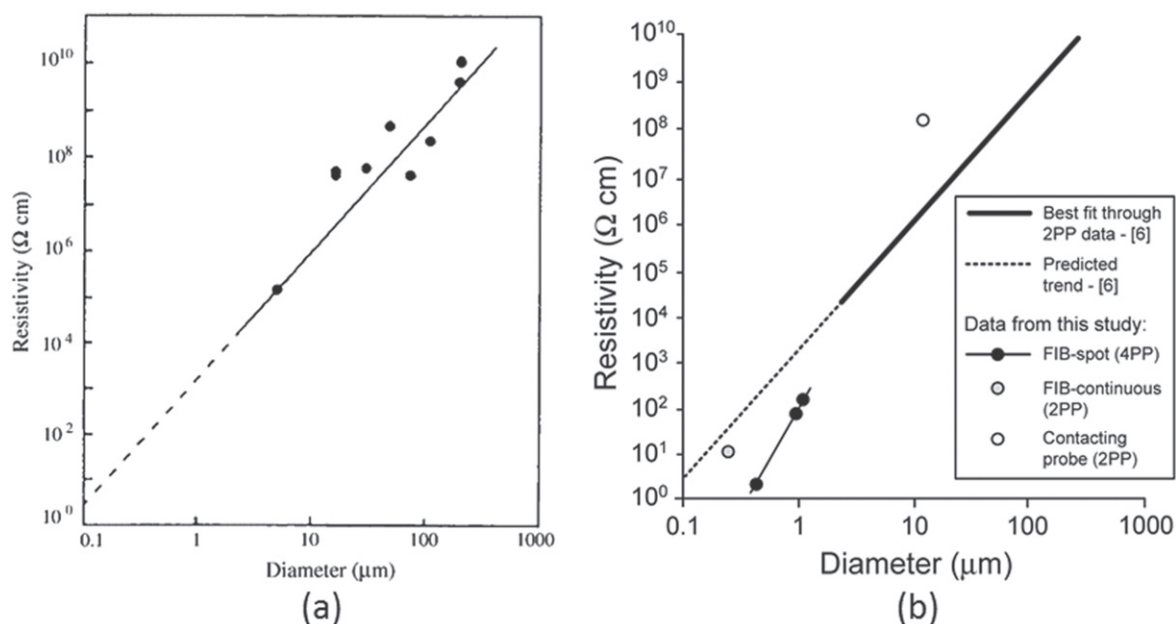


Figure 5. Electrical resistivity of C_{60} whiskers measured as a function of diameter. The resistivity measurement was performed by the two-point probe method (2PP) in (a) and by the four-point probe method (4PP) in (b). [6] in the inset of (b) is identical with [70]. FIB stands for focused ion beam. Part (a) reprinted with permission from [70], copyright © 2003 John Wiley & Sons, Ltd. Part (b) reproduced by permission of ECS—The Electrochemical Society from [71]

The electrical resistivity of C_{60} whiskers with diameters greater than $1 \mu\text{m}$ (~ 10 –a few hundred micrometers) was measured using a two-terminal method at ambient temperature [70]. The electrical resistivity of the C_{60} whiskers decreased dramatically with decreasing diameter (figure 5(a)). The resistivity of C_{60} NWs is expected to be several Ohm centimeters ($\Omega \text{ cm}$), based on extrapolation of the curve-fitted data. Subsequently, Larsson *et al* measured the electrical resistivity using a four-point probe method [71]. Figure 5(b) summarizes their results including figure 5(a) [70]. The four-point probe method also showed a decrease in resistivity of C_{60} whiskers with decreasing diameter (FIB-spot (4PP)), figure 5(b)). A C_{60} NW with a diameter of 650 nm showed a low resistivity of $3 \Omega \text{ cm}$ [71]. The decrease in resistivity with decreasing diameter suggested that C_{60} NWs with smaller diameters and shorter C_{60} intermolecular distances are more crystalline and thus have a greater overlap of π electrons [70]. Recently, this fact was further confirmed by Barzegar *et al* using thinner C_{60} NWs [93]. It was shown that the electrical mobility of as-grown C_{60} NWs with diameters less than 300 nm increases with decreasing the diameter of C_{60} NWs [64, 93–95].

If the line measured using the four-point probe method is extrapolated to a diameter of 100 nm in figure 5(b), the resistivity will decrease to the order of $10^{-3} \Omega \text{ cm}$. This result suggests that C_{60} NWs may exhibit metallic conductivity when their diameters are sufficiently small. Xu *et al* showed that C_{60} NWs are conductive only if the surface is not covered by oxygen [72].

To determine the electrical properties of a semiconductor, it is necessary to measure the temperature dependence of

electrical conductivity. Ji *et al* performed these measurements using C_{60} NWs with either a face-centered cubic (fcc) or a hexagonal closed packed (hcp) structure [73]. The fcc C_{60} NW displayed higher electrical conductivity than did the hcp C_{60} NW. This result confirms that the crystal structure influences the electrical properties of C_{60} NWs. However, the effect of solvent molecules contained in the hcp C_{60} NW is still under some debate. If C_{60} molecules adopt a closely packed structure, a greater overlap between π electrons would lead to higher electrical conductivity in these C_{60} NWs [70, 73].

Carbon superconductors have been investigated for many years. The superconductivity of graphite (C_8) specimens doped with alkali metals, including K (superconducting transition temperature (T_c) $< 0.55 \text{ K}$ [74], 0.128 – 0.198 K [75]), Cs ($T_c = 0.020$ – 0.135 K [74]), and Rb ($T_c = 0.023$ – 0.151 K [74]) has been reported. Graphite superconductors such as $C_6\text{Ca}$ ($T_c = 11.5 \text{ K}$) and $C_6\text{Yb}$ ($T_c = 6.5 \text{ K}$) were also synthesized [76]. C_{60} NWs can be transformed into glassy carbon nanofibers by heat treatment [77–79]. When heated to $3000 \text{ }^\circ\text{C}$, C_{60} NWs transform into carbon nanofibers with up to 17 graphene layers [77]. The number of stacked graphene layers increases with increasing temperature between 2000 and $3000 \text{ }^\circ\text{C}$ [77]. Those C_{60} NWs heated at high temperatures with developed graphitic ribbons are promising materials that may exhibit superconductivity if doped with alkali metals and alkaline-earth metals. In addition, the high-temperature-treated C_{60} NWs become electron emission tips showing striped patterns that reflect the atomic structure of the crumpled graphitic layers [78, 79]. However, since long amorphous carbon nanofibers prepared by high-

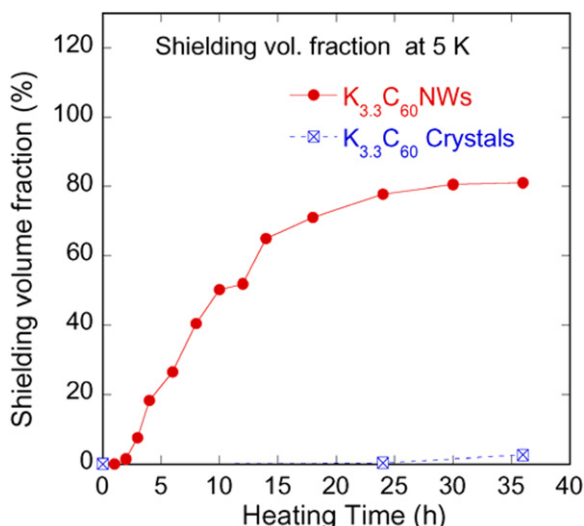


Figure 6. Shielding volume fractions in K-doped C_{60} NWs and K-doped C_{60} crystal powder (reprinted from [87]).

temperature heat treatment of C_{60} NWs showed cytotoxicity like long multiwall carbon nanotubes [96], special care will be necessary in the practical uses of the glassy carbon nanofibers.

In 2004, boron-doped diamond was observed to exhibit superconductivity ($T_c \approx 4$ K) [80]. Takano *et al* found that the T_c of a boron-doped diamond film was 7.4 K [81].

Hebard *et al* discovered that C_{60} doped with potassium (K) exhibited superconductivity [82]. A superconducting transition temperature (T_c) of 18 K was observed for both K-doped C_{60} films and bulk samples. Tanigaki *et al* reported the highest T_c value of 33 K in $Cs_2Rb_1C_{60}$ powder [83].

Of the three known phases of K-doped C_{60} (fcc (K_3C_{60}), body-centered tetragonal (bct) (K_4C_{60}), and body-centered cubic (bcc) (K_6C_{60})), only the fcc phase exhibits superconductivity [84]. Although C_{60} NWs that are grown in solution display a solvated hexagonal structure, they transform into an fcc structure upon drying and removal of the internal solvent molecules [85]. Hence, these fcc C_{60} NWs should be superconducting if doped with alkali metals [15]. C_{60} nanotubes were doped with Li, Na, and K, and the crystal structures were examined using Raman spectroscopy [86]. Superconductive C_{60} NWs were also successfully fabricated by doping with K [87, 88]. Although the T_c value (17 K) of the K-doped C_{60} NWs with a nominal composition of $K_{3.3}C_{60}$ was lower than the reported value of 18 K [82], the superconducting, shielding volume fraction was as high as 80%, and the critical current density J_c was more than 3×10^5 A cm⁻² under 50 kOe [87, 88], although the doping was performed at 200 °C for 24 h. The shielding volume fraction of the K-doped C_{60} crystal powder was less than 1% when doped using the same process (figure 6). The high shielding volume fraction in the K-doped C_{60} NWs may allow for light, flexible, and recyclable superconducting carbon cables. Initially, the superconducting shielding volume fraction of K-doped C_{60} crystals was at most 35%, even after

prolonged heat treatment (20 days) at temperatures up to 250 °C [89].

Efforts to increase the T_c value of alkali-doped C_{60} NWs are continuing. Values up to 26 K have been achieved by doping with Rb [90]. The volume fraction of Rb-doped C_{60} NWs was approximately five times greater than that of Rb-doped C_{60} powder. As Rb is an abundant alkali metal like the other common metals such as copper, lead, or zinc [91], lightweight Rb-doped C_{60} NWs are expected to find use in a variety of superconducting applications, including motor cars, cables for power delivery, and wind generators.

4. Summary

A variety of fullerene nanofibers and nanosheets have been synthesized using LLIP methods. These materials have found use in a wide range of applications, including solar cells, chemical sensors, photo sensors, photocatalysts, and ambipolar field-effect transistors. The synthesis of C_{60} NWs using a dynamic LLIP method with a C_{60} -saturated toluene solution and IPA suggests that nucleation is governed by the volume of the liquid–liquid interface produced by interdiffusion between the two solvents.

Alkali-metal-doped C_{60} NWs are the first carbon fibers to display superconductivity while being lightweight and flexible. K- or Rb-doped C_{60} NWs are promising superconductors with T_c values that are higher than those of any other practically used metal superconductors. Additionally, they are composed of non-toxic, abundant, and recyclable elements. Fullerene nanomaterials show great promise for a variety of applications in electrical and optical fields.

Acknowledgments

This research was supported by the Health and Labour Sciences Research Grants (H24-Chemistry-Shitei-009) from the Ministry of Health, Labour and Welfare of Japan, the JST Strategic Japanese-EU Cooperative Program ‘Study on managing the potential health and environmental risks of engineered nanomaterials’, the Center of Materials Research for Low Carbon Emission of the National Institute for Materials Science, and the Japan Society for the Promotion of Science KAKENHI Grant No. 26600007.

References

- [1] Kroto H W, Heath J R, O’Brien S C, Curl R F and Smalley R E 1985 C_{60} : buckminsterfullerene *Nature* **318** 162–3
- [2] Okada S, Saito S and Oshiyama A 1999 New metallic crystalline carbon: three dimensionally polymerized C_{60} fullerite *Phys. Rev. Lett.* **83** 1986
- [3] Rao A M *et al* 1993 Photoinduced polymerization of solid C_{60} film *Science* **259** 955–7
- [4] Kato R and Miyazawa K 2012 Raman laser polymerization of C_{60} nanowhiskers *J. Nanotechnol.* **2012** 101243

- [5] Iwasa Y *et al* 1994 New phases of C₆₀ synthesized at high pressure *Science* **264** 1570
- [6] Miyazawa K, Satsuki H, Kuwabara M and Akaishi M 2001 Microstructural analysis of high-pressure compressed C₆₀ *J. Mater. Res.* **16** 1960–6
- [7] Minato J, Miyazawa K, Suga T, Kanda H, Akaishi M, Yamaura K, Muromachi E and Kakisawa H 2005 Characterization of high-pressure sintered C₆₀ nanowhiskers and C₆₀ powder *J. Mater. Res.* **20** 742–6
- [8] Miyazawa K, Akaishi M, Kuwasaki Y and Suga T 2003 Characterizing high-pressure compressed C₆₀ whiskers and C₆₀ powder *J. Mater. Res.* **18** 166–72
- [9] Nakaya M, Nakayama T and Aono M 2004 Fabrication and electron-beam-induced polymerization of C₆₀ nanoribbon *Thin Solid Films* **464–5** 327–30
- [10] Miyazawa K, Minato J, Fujino M and Suga T 2006 Structural investigation of heat-treated fullerene nanotubes and nanowhiskers *Diam. Relat. Mater.* **15** 1143–6
- [11] Popov M, Mordkovich V, Perfilov S, Kirichenko A, Kulnitskiy B, Perezhugin I and Blank V 2014 Synthesis of ultrahard fullerite with a catalytic 3D polymerization reaction of C₆₀ *Carbon* **76** 250–6
- [12] Blank V, Popov M, Pivovarov G, Lvova N, Gogolinsky K and Reshetov V 1998 Ultrahard and superhard phases of fullerite C₆₀: comparison with diamond on hardness and wear *Diam. Relat. Mater.* **7** 427–31
- [13] Miyazawa K, Obayashi A and Kuwabara M 2001 C₆₀ nanowhiskers in a mixture of lead zirconate titanate sol–C₆₀ toluene solution *J. Am. Ceram. Soc.* **84** 3037–9
- [14] Rauwerdink K, Liu J, Kintigh J and Miller G P 2007 Thermal, sonochemical, and mechanical behaviors of single crystal [60] fullerene nanotubes *Microsc. Res. Tech.* **70** 513–21
- [15] Miyazawa K and Kuwabara M 2005 Fine carbon wires and methods for producing the same *US Patent* 6890505B2
- [16] Miyazawa K 2009 Synthesis and properties of fullerene nanowhiskers and fullerene nanotubes *J. Nanosci. Nanotechnol.* **9** 41–50
- [17] Miyazawa K (ed) 2011 *Fullerene Nanowhiskers* (Singapore: Pan Stanford Publishing Pte. Ltd)
- [18] Wakahara T, Nemoto Y, Xu M, Miyazawa K and Fujita D 2010 Preparation of endohedral metallofullerene nanowhiskers and nanosheets *Carbon* **48** 3359–63
- [19] Miyazawa K, Minato J, Mashino T, Nakamura S, Fujino M and Suga T 2006 Structural characterization of room-temperature synthesized fullerene nanowhiskers *Nukleonika* **51** (Suppl. 1) S41–8
- [20] Miyazawa K, Mashino T and Suga T 2004 Liquid phase synthesis of the nanowhiskers of fullerene derivatives *Trans. Mater. Res. Soc. Japan* **29** 537–40
- [21] Miyazawa K, Mashino T and Suga T 2003 Structural characterization of the C₆₀[C(COOC₂H₅)₂] whiskers prepared by the liquid–liquid interfacial precipitation method *J. Mater. Res.* **18** 2730–5
- [22] Miyazawa K and Suga T 2004 Transmission electron microscopy investigation of fullerene nanowhiskers and needle-like precipitates formed by using C₆₀ and (η²-C₆₀)Pt(PPh₃)₂ *J. Mater. Res.* **19** 2410–4
- [23] Miyazawa K, Minato J, Yoshii T, Fujino M and Suga T 2005 Structural characterization of the fullerene nanotubes prepared by the liquid–liquid interfacial precipitation method *J. Mater. Res.* **20** 688–95
- [24] Miyazawa K and Ringor C 2008 Platinum chloride deposition into C₆₀ nanotubes *Mater. Lett.* **62** 410–3
- [25] Kizuka T, Miyazawa K and Tokumine T 2012 Young's modulus of single-crystal fullerene C₇₀ nanotubes *J. Nanotechnol.* **2012** 969357
- [26] Liu H *et al* 2002 Imaging as-grown [60] fullerene nanotubes by template technique *J. Am. Chem. Soc.* **124** 13370–1
- [27] Zhang X, Qu Y, Piao G, Zhao J and Jiao K 2010 Reduced working electrode based on fullerene C₆₀ nanotubes@DNA: characterization and application *Mater. Sci. Eng. B* **175** 159–63
- [28] Kizuka T, Miyazawa K and Tokumine T 2012 Synthesis of oriented bundle fibers of fullerene C₇₀ crystal nanotubes *J. Nanosci. Nanotechnol.* **12** 2825–8
- [29] Miyazawa K, Fujino M, Minato J, Yoshii T, Kizuka T and Suga T 2004 Structure and properties of fullerene nanowhiskers prepared by the liquid–liquid interfacial precipitation method *Proc. SPIE* **5648** 224
- [30] Miyazawa K, Kuwasaki Y, Obayashi A and Kuwabara M 2002 C₆₀ nanowhiskers formed by the liquid–liquid interfacial precipitation method *J. Mater. Res.* **17** 83–8
- [31] Osonoe K, Kano R, Miyazawa K and Tachibana M 2014 Synthesis of C₇₀ two-dimensional nanosheets by liquid–liquid interfacial precipitation method *J. Cryst. Growth* **401** 458–461
- [32] Wakahara T, Sathish M, Miyazawa K, Hu C, Tateyama Y, Nemoto Y, Sasaki T and Ito O 2009 Preparation and optical properties of fullerene/ferrocene hybrid hexagonal nanosheets and large-scale production of fullerene hexagonal nanosheets *J. Am. Chem. Soc.* **131** 9940–4
- [33] Shrestha L K, Sathish M, Hill J P, Miyazawa K, Tsuruoka T, Sanchez-Ballester N M, Honma I, Ji Q and Ariga K 2013 Alcohol-induced decomposition of Olmstead's crystalline Ag(I)-fullerene heteronanostructure yields 'bucky cubes' *J. Mater. Chem. C* **1** 1174–81
- [34] Shrestha L K, Hill J P, Tsuruoka T, Miyazawa K and Ariga K 2013 Surfactant-assisted assembly of fullerene (C₆₀) nanorods and nanotubes formed at a liquid–liquid interface *Langmuir* **29** 7195–202
- [35] Shrestha L K, Ji Q, Mori T, Miyazawa K, Yamauchi Y, Hill J P and Ariga K 2013 Fullerene nanoarchitectonics: from zero to higher dimensions *Chem. Asian J.* **8** 1662–79
- [36] Shrestha L K, Yamauchi Y, Hill J P, Miyazawa K and Ariga K 2013 Fullerene crystals with bimodal pore architectures consisting of macropores and mesopores *J. Am. Chem. Soc.* **135** 586–9
- [37] Shrestha L K, Hill J P, Miyazawa K and Ariga K 2012 Mixing antisolvents induced modulation in the morphology of crystalline C₆₀ *J. Nanosci. Nanotechnol.* **12** 6380–4
- [38] Sathish M and Miyazawa K 2007 Size-tunable hexagonal fullerene (C₆₀) nanosheets at liquid–liquid interface *J. Am. Chem. Soc.* **129** 13816–7
- [39] Miyazawa K and Hotta K 2010 The effect of solvent ratio and water on the growth of C₆₀ nanowhiskers *J. Cryst. Growth* **312** 2764–70
- [40] Cha S I, Miyazawa K and Kim J-D 2008 Vertically well-aligned C₆₀ micro-tube crystal array prepared using solution-based one step process *Chem. Mater.* **20** 1667–9
- [41] Miyazawa K, Minato J, Mashino T, Yoshii T, Kizuka T, Kato R, Tachibana M and Suga T 2005 Characterization of the liquid-phase synthesized fullerene nanotubes and nanowhiskers *Proc. of the 2nd JSME/ASME Int. Conf. on Materials and Processing 2005—M&P2005: The 13th JSME Materials and Processing Conf. (Seattle, WA, 19–22 June)* pp (SMS23)-1–4
- [42] Miyazawa K, Kuriyama R, Shimomura S, Wakahara T and Tachibana M 2014 Growth and FIB-SEM analyses of C₆₀ microtubes vertically synthesized on porous alumina membranes *J. Cryst. Growth* **388** 5–11
- [43] Cha S I, Miyazawa K and Kim J 2014 Substrate having fullerene thin wires and method for manufacture thereof *United States Patent* 8685160B2
- [44] Amer M S, Todd T K and Busbee J D 2011 Effect of linear alcohol molecular size on the self-assembly of fullerene whiskers *Mater. Chem. Phys.* **130** 90–4

- [45] Hotta K and Miyazawa K 2008 Growth rate measurement of C₆₀ fullerene nanowhiskers *Nano* **3** 355–9
- [46] Asaka K, Kato R, Yoshizaki R, Miyazawa K and Kizuka T 2007 Fracture surface and correlation of buckling force with aspect ratio of C₆₀ crystalline whiskers *Diam. Relat. Mater.* **16** 1936–9
- [47] Kizuka T, Saito K and Miyazawa K 2008 Young's modulus of crystalline C₆₀ nanotubes studied by *in situ* transmission electron microscopy *Diam. Relat. Mater.* **17** 972–4
- [48] Saito K, Miyazawa K and Kizuka T 2009 Bending process and Young's modulus of fullerene C₆₀ nanowhiskers *Japan. J. Appl. Phys.* **48** 010217
- [49] Asaka K, Kato R, Miyazawa K and Kizuka T 2006 Buckling of C₆₀ whiskers *Appl. Phys. Lett.* **89** 071912
- [50] Kato R and Miyazawa K 2011 Cross-sectional structural analysis of C₆₀ nanowhiskers by transmission electron microscopy *Diam. Relat. Mater.* **20** 299–303
- [51] Kizuka T, Miyazawa K and Tokumine T 2012 Solvation-assisted Young's modulus control of single-crystal fullerene C₇₀ nanowhiskers *J. Nanotechnol.* **2012** 583817
- [52] Miyazawa K, Hamamoto K, Nagata S and Suga T 2003 Structural investigation of the C₆₀/C₇₀ whiskers fabricated by forming liquid–liquid interfaces of toluene with dissolved C₆₀/C₇₀ and isopropyl alcohol *J. Mater. Res.* **18** 1096–103
- [53] Minato J, Miyazawa K and Suga T 2005 Morphology of C₆₀ nanotubes fabricated by the liquid–liquid interfacial precipitation method *Sci. Technol. Adv. Mater.* **6** 272–7
- [54] Ji H-X, Hu J-S, Tang Q-X, Song W-G, Wang C-R, Hu W-P, Wan L-J and Lee S-T 2007 Controllable preparation of submicrometer single-crystal C₆₀ rods and tubes through concentration depletion at the surfaces of seeds *J. Phys. Chem. C* **111** 10498–502
- [55] Ringor C L and Miyazawa K 2009 Fabrication of solution grown C₆₀ fullerene nanotubes with tunable diameter *J. Nanosci. Nanotechnol.* **9** 6560–4
- [56] Hotta K and Miyazawa K 2008 Growth rate measurement of C₆₀ fullerene nanowhiskers *Nano* **3** 355–9
- [57] Tachibana M, Kobayashi K, Uchida T, Kojima K, Tanimura M and Miyazawa K 2003 Photo-assisted growth and polymerization of C₆₀ 'nano' whiskers *Chem. Phys. Lett.* **374** 279–85
- [58] Kobayashi K, Tachibana M and Kojima K 2005 Photo-assisted growth of C₆₀ nanowhiskers from solution *J. Cryst. Growth* **274** 617–21
- [59] Miyazawa K and Hotta K 2011 The effect of water on the stability of C₆₀ fullerene nanowhiskers *J. Nanopart. Res.* **13** 5739–47
- [60] Wei M, Luo H, Li N, Zhang S and Gan L 2002 Study of electrochemical properties of pyrrolidinofullerenes by microelectrode voltammetry *Microchem. J.* **72** 115–112
- [61] Wakahara T, Miyazawa K, Nemoto Y and Ito O 2011 Diameter controlled growth of fullerene nanowhiskers and their optical properties *Carbon* **49** 4644–9
- [62] Miyazawa K, Hirata C and Wakahara T 2014 Influence of the solution volume on the growth of C₆₀ nanowhiskers *J. Cryst. Growth* **405** 68–72
- [63] Kawasaki S and Sakai E 1967 Measurement of diffusion of gold in copper by elastic scattering of deuteron *J. Nucl. Sci. Technol.* **4** 273–7
- [64] Ogawa K, Kato T, Ikegami A, Tsuji H, Aoki N and Ochiai Y 2006 Electrical properties of field-effect transistors based on C₆₀ nanowhiskers *Appl. Phys. Lett.* **88** 112109
- [65] Somani P R, Somani S P and Umeno M 2007 Toward organic thick film solar cells: three dimensional bulk heterojunction organic thick film solar cell using fullerene single crystal nanorods *Appl. Phys. Lett.* **91** 173503
- [66] Shrestha R G, Shrestha L K, Khan A H, Kumar G S, Acharya S and Ariga K 2014 Demonstration of ultrarapid interfacial formation of 1D fullerene nanorods with photovoltaic properties *Appl. Mater. Interfaces* **6** 15597–603
- [67] Cho B H, Lee K B, Miyazawa K and Ko W B 2013 Preparation of fullerene (C₆₀) nanowhisker-ZnO nanocomposites by heat treatment and photocatalytic degradation of methylene blue *Asian J. Chem.* **25** 8027–30
- [68] Yang J, Lim H, Choi H C and Shin H S 2010 Wavelength-selective silencing of photocurrent in Au-coated C₆₀ wire hybrid *Chem. Commun.* **46** 2575–7
- [69] Li H, Tee B C-K, Cha J J, Cui Y, Chung J W, Lee S Y and Bao Z 2012 High-mobility field-effect transistors from large-area solution-grown aligned C₆₀ single crystals *J. Am. Chem. Soc.* **134** 2760–5
- [70] Miyazawa K, Kuwasaki Y, Hamamoto K, Nagata S, Obayashi A and Kuwabara M 2003 Structural characterization of the C₆₀ nanowhiskers formed by the liquid–liquid interfacial precipitation method *Surf. Interface Anal.* **35** 117–20
- [71] Larsson M P, Kjelstrup-Hansen J and Lucyszyn S 2007 Dc characterisation of C₆₀ whiskers and nanowhiskers *ECS Trans.* **2** 27–38
- [72] Xu M S, Pathak Y, Fujita D, Ringor C and Miyazawa K 2008 Covered conduction of individual C₆₀ nanowhiskers *Nanotechnology* **19** 075712
- [73] Ji H-X, Hu J-S, Wan L-J, Tang Q-X and Hu W-P 2008 Controllable crystalline structure of fullerene nanorods and transport properties of an individual nanorod *J. Mater. Chem.* **18** 328–32
- [74] Hannay N B, Geballe T H, Matthias B T, Andres K, Schmidt P and MacNair D 1965 Superconductivity in graphitic compounds *Phys. Rev. Lett.* **14** 225–6
- [75] Koike Y, Suematsu H, Higuchi K and Tanuma S 1980 Superconductivity in graphite–alkali metal intercalation compounds *Physica B* **99** 503–8
- [76] Weller T E, Ellerby M, Saxena S S, Smith R P and Skipper N T 2005 Superconductivity in the intercalated graphite compounds C₆Yb and C₆Ca *Nat. Phys.* **1** 39–41
- [77] Kato R, Miyazawa K, Nishimura T and Wang Z M 2009 High-resolution transmission electron microscopy of heat-treated C₆₀ nanotubes *J. Phys.: Conf. Ser.* **159** 012024
- [78] Asaka K, Nakayama T, Miyazawa K and Saito Y 2012 Study on structure of heat-treated fullerene nanowhiskers and their field electron emission characteristics *Surf. Interface Anal.* **44** 780–3
- [79] Asaka K, Nakayama T, Miyazawa K and Saito Y 2012 Structures and field emission properties of heat-treated C₆₀ fullerene nanowhiskers *Carbon* **50** 1209–15
- [80] Ekimov E A, Sidorov V A, Bauer E D, Mel'nik N N, Curro N J, Thompson J D and Stishov S M 2004 Superconductivity in diamond *Nature* **428** 542–5
- [81] Takano Y, Nagao M, Sakaguchi I, Tachiki M, Hatano T, Kobayashi K, Umezawa H and Kawarada H 2004 Superconductivity in diamond thin films well above liquid helium temperature *Appl. Phys. Lett.* **85** 2851–3
- [82] Hebard A F, Rosseinsky M J, Haddon R C, Murphy D W, Glarum S H, Palstra T T M, Ramirez A P and Kortan A R 1991 Superconductivity at 18 K in potassium-doped C₆₀ *Nature* **350** 600
- [83] Tanigaki K, Ebbesen T W, Saito S, Mizuki J, Tsai J S, Kubo Y and Kuroshima S 1991 Superconductivity at 33 K in C₈Rb₃C₆₀ *Nature* **352** 222–3
- [84] Haddon R C 1992 Electronic structure, conductivity, and superconductivity of alkali metal doped C₆₀ *Acc. Chem. Res.* **25** 127–33
- [85] Minato J and Miyazawa K 2005 Solvated structure of C₆₀ nanowhiskers *Carbon* **43** 2837–41
- [86] Cui W *et al* 2011 Synthesis of alkali-metal-doped C₆₀ nanotubes *Diam. Relat. Mater.* **20** 93–6

- [87] Takeya H, Miyazawa K, Kato R, Wakahara T, Ozaki T, Okazaki H, Yamaguchi T and Takano Y 2012 Superconducting fullerene nanowhiskers *Molecules* **17** 4851–9
- [88] Takeya H, Kato R, Wakahara T, Miyazawa K, Yamaguchi T, Ozaki T, Okazaki H and Takano Y 2013 Preparation and superconductivity of potassium-doped fullerene nanowhiskers *Mater. Res. Bull.* **48** 343–5
- [89] Murphy D W, Rosseinsky M J, Haddon R C, Ramirez A P, Hebard A F, Tycko R, Fleming R M and Dabbagh G 1991 Superconductivity in alkali metal fullerenes *Physica C* **185–9** 403–7
- [90] Takeya H, Miyazawa K and Takano Y 2012 Development of alkali-metal doped superconducting fullerene nanowhiskers *Mater. Integr.* **25** 38–44 (in Japanese)
- [91] Buttermann W C and Reese R G Jr 2003 *Mineral Commodity Profiles—Rubidium (US Geological Survey Open-File Report 03-045)*
- [92] Wakahara T, Angelo P D', Miyazawa K, Nemoto Y and Ito O 2012 Fullerene/cobalt porphyrin hybrid nanosheets with ambipolar charge transporting characteristics *J. Am. Chem. Soc.* **134** 7204–6
- [93] Barzegar H R, Larsen C, Edman L and Wågberg T 2013 Solution-based phototransformation of C₆₀ nanorods: towards improved electronic devices *Part. Part. Syst. Charact.* **30** 715–20
- [94] Larsen C, Barzegar H R, Nitze F, Wågberg T and Edman L 2012 On the fabrication of crystalline C₆₀ nanorod transistors from solution *Nanotechnology* **23** 344015
- [95] Doi T, Koyama K, Chiba Y, Tsuji H, Ueno M, Chen S-R, Aoki N, Bird J P and Ochiai Y 2010 Electron transport properties in photo and supersonic wave irradiated C₆₀ fullerene nano-whisker field-effect transistors *Japan. J. Appl. Phys.* **49** 04DN12
- [96] Cui H *et al* 2014 High-temperature calcined fullerene nanowhiskers as well as long needle-like multi-wall carbon nanotubes have abilities to induce NLRP3-mediated IL-1 β secretion *Biochem. Biophys. Res. Commun.* **452** 593–9